Materials Science and Engineering A362 (2003) 2–16

www.elsevier.com/locate/msea

Cracks in functionally graded materials☆

H.-A. Bahr[a], H. Balke[a], T. Fett[b], I. Hofinger[a], G. Kirchhoff[c], D. Munz[b,*], A. Neubrand[d], A.S. Semenov[a], H.-J. Weiss[c], Y.Y. Yang[b]

[a] *Department of Mechanical Engineering, Dresden University of Technology, Dresden 01062, Germany*
[b] *Institut für Materialforschung, Forschungszentrum Karlsruhe, Karlsruhe 76021, Germany*
[c] *Fraunhofer Institute for Material and Beam Technology, Winterbergstrasse 28, Dresden 01277, Germany*
[d] *Department of Materials Science, University of Technology Darmstadt, Darmstadt 64297, Germany*

Received 18 July 2002; received in revised form 29 November 2002

Abstract

The weight function method is described to analyze the crack growth behavior in functionally graded materials and in particular materials with a rising crack growth resistance curve. Further, failure of graded thermal barrier coatings (TBCs) under cyclic surface heating by laser irradiation is modeled on the basis of fracture mechanics. The damage of both graded and non-graded TBCs is found to develop in several distinct stages: vertical cracking → delamination → blistering → spalling. This sequence can be understood as an effect of progressive shrinkage due to sintering and high-temperature creep during thermal cycling, which increases the energy-release rate for vertical cracks which subsequently turn into delamination cracks. The results of finite element modeling, taking into account the TBC damage mechanisms, are compatible with experimental data. An increase of interface fracture toughness due to grading and a decrease due to ageing have been measured in a four-point bending test modified by a stiffening layer. Correlation with the damage observed in cyclic heating is discussed. It is explained in which way grading is able to reduce the damage.

Keywords: FGM; Fracture mechanics; *R*-curve; Residual stresses; TBC

1. Introduction

Replacing the sharp transition of the material properties in a bimaterial joint by a continuous transition, i.e. introduction of a graded interlayer, may improve the strength of the joint. Various arguments have been mentioned in literature, according to which a graded material should be beneficial. These arguments are (see e.g. [1]) that: (i) thermal stresses can be reduced; (ii) thermal stresses at critical locations can be reduced; (iii) stress jumps at the interface can be avoided; (iv) the driving force for crack extension, the stress intensity factor, can be reduced; and (v) the strength of the interfacial bond, which may be characterized by the interfacial fracture toughness, can be increased.

Not all these arguments are convincing. The reduction of thermal stresses depends strongly on the thickness of the interlayer and the mechanical boundary conditions. A thin interlayer between two different materials or a thin coating contributes only negligibly to the equilibrium conditions of force and moment and therefore leads to a small change in the stress distribution only. On the other hand, a continuous linear gradation in a plate leads to zero thermal stress, if free bending of the plate is possible. If, however, the plate is constrained against bending, a linear gradation leads to a change in the thermal stresses, but not to a general reduction in the stresses. This is shown in Fig. 1, where the dimensionless stress $\sigma/E_1\alpha_1\Delta T$ is plotted versus the coordinate y in the direction of the gradation. E_1 and α_1 are the Young's modulus and the thermal expansion coefficient for $y = 0$, E_2 and α_2 are the corresponding values for $y = H$, and ΔT is the change of the temperature from the stress free state.

☆ This is an overview of parts of the key results obtained within the priority program "Functionally Graded Materials" funded by the German Research Foundation (DFG) in the years 1995–2000.

* Corresponding author. Present address: Institut fur Zuverlassigkeit im Maschinenbau, Universitat Karlsruhe (TH), Postfach 3640, Karlsruhe 76021, Germany. Tel.: +49-7247-82-4894; fax: +49-7247-82-2347.
E-mail address: munz@imf.fzk.de (D. Munz).

0921-5093/$ – see front matter © 2003 Published by Elsevier B.V.
doi:10.1016/S0921-5093(03)00582-3

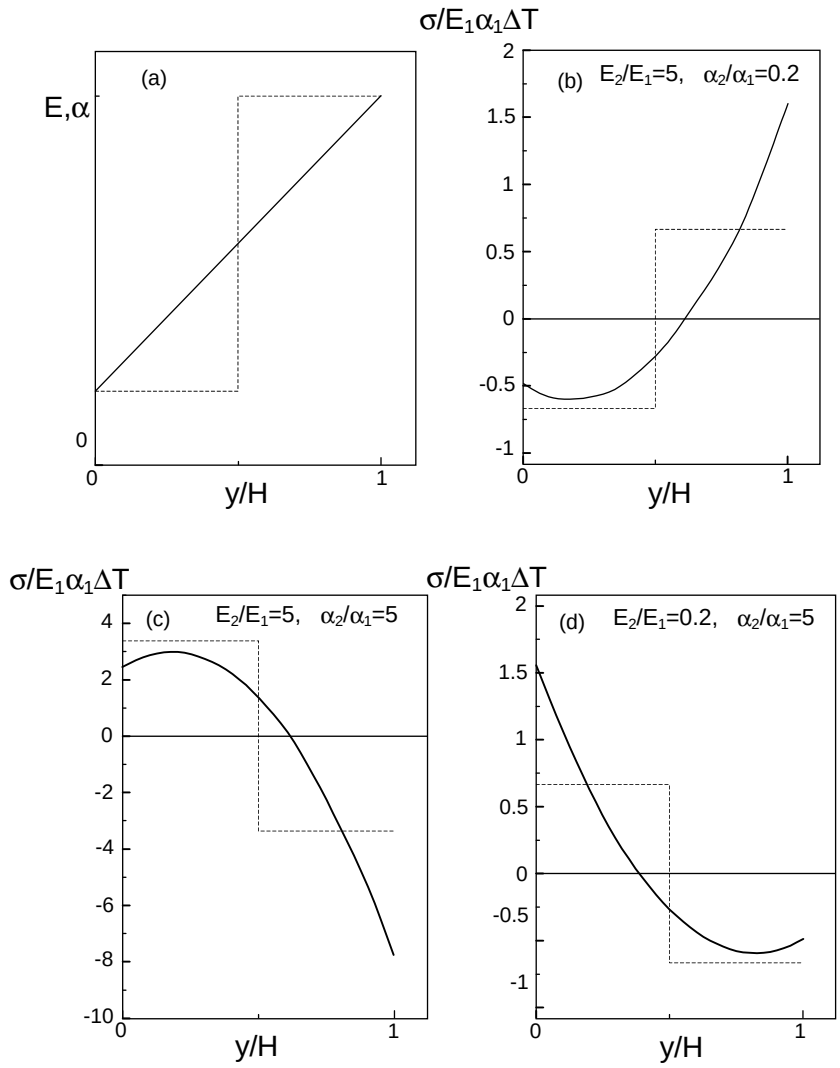

Fig. 1. Stress distribution in a plate constraint against bending after a change in temperature (linear gradation and bimaterial).

The jump of the stress in a bimaterial is not necessarily dangerous, because failure is caused by stresses and not by changes in the stresses. If there are flaws, such as voids or inclusions or an irregular boundary at the interface, the jump in the stress may lead to locally high stresses [2].

In a 6-year program of the German Science Foundation, different aspects of functionally graded materials were investigated. One aspect was the mechanical properties of these materials. Results were published in different papers [3–6].

This paper concentrates on cracks in functionally graded materials. There exist many publications on cracks in functionally graded materials under mechanical and thermal loading [7–35]. Section 2 of this paper deals with the application of the weight function method to calculate stress intensity factors, with the analysis of the rising crack growth resistance and with residual stresses. In Section 3, the effect of grading on delamination crack propagation in TBCs under heating by means of laser irradiation is analyzed.

2. Weight function analysis

2.1. Weight functions for the calculation of stress intensity factors

The stresses at the tip of cracks in a graded material are described in the same way as in homogeneous materials with a square root singularity. For cracks parallel to the gradation direction an external mode I loading leads to a mode I stress intensity factor, whereas for a crack perpendicular to the direction of the gradation an external mode I loading leads to mixed mode K_I/K_{II} loading. The stress intensity factor depends on the applied stress but also on the distribution of the elastic constants, especially the Young's modulus.

A crack of length "a" parallel to the gradation direction (y-direction) is considered. The stress intensity factors can be calculated applying the weight function method:

$$K_I = \int_0^a \sigma(y) h_I(y, a)\, dy \tag{1a}$$

$$K_{II} = \int_0^a \tau(y) h_{II}(y, a)\, dy \tag{1b}$$

where $\sigma(y)$ and $\tau(y)$ are the normal and shear stress distributions in the uncracked component along the crack plane. The h_I and h_{II} are the mode I and mode II weight functions. For a graded material these weight functions depend on the distribution of the elastic constants $E(y)$ and $\nu(y)$.

Rice [36] developed a relation to calculate the weight function from the crack opening displacement $u(y, a)$, the stress intensity factor $K_r(a)$ of a reference stress distribution $\sigma_r(y)$:

$$h_I(y, a) = \frac{E}{K_{Ir}} \frac{\partial u(y, a)}{\partial a}. \tag{2}$$

It can be shown [37] that the same relation holds for a crack in a graded material, where $E(a)$ at the tip of the crack has to be introduced for the Young's modulus. To obtain the crack opening displacement, a procedure developed for homogeneous materials (see [38]) can be applied. This was shown in [37]. The "direct adjustment method" [39] starts with the general type of the weight function

$$h(y, a) = \sqrt{\frac{2}{\pi a}} \left[\frac{1}{\sqrt{1-\rho}} + \sum_{n=1}^{\infty} D_n (1-\rho)^{n-1/2} \right] \tag{3}$$

with $\rho = y/a$. The expansion is truncated after a certain number N. D_n can be obtained from N conditions. One set of conditions can be obtained by applying Eq. (1) for reference loading $\sigma_r(y)$ with known stress intensity factors $K_r(a)$. Another condition was obtained in [37,40]. It could be shown that the second derivative of the crack opening displacement at the crack mouth ($x = 0$) disappears. As a direct consequence of Eq. (2) it follows

$$\frac{\partial^2 h}{\partial y^2}\Big|_{y=0} = 0 \tag{4}$$

As an example, a component with an external crack is considered. Two reference loadings are considered: a constant crack face pressure $\sigma(y) =$ constant and a pair of concentrated forces P acting at the crack mouth, leading to the stress intensity factors K_σ and K_P. With these three conditions, a four-term weight function can be obtained

$$h(y, a) = \sqrt{\frac{2}{\pi a}} \left[\frac{1}{\sqrt{1-\rho}} + D_1(1-\rho)^{1/2} + D_2(1-\rho)^{3/2} + D_3(1-\rho)^{5/2} \right]. \tag{5}$$

The three conditions lead to

$$\frac{K_\sigma}{\sigma} = \sqrt{\frac{2a}{\pi}} \left(2 + \tfrac{2}{3} D_1 + \tfrac{2}{5} D_2 + \tfrac{2}{7} D_3\right) \tag{6a}$$

$$\frac{K_P}{P} = \sqrt{\frac{2}{\pi a}} (1 + D_1 + D_2 + D_3) \tag{6b}$$

$$3 - D_1 + 3D_2 + 15D_3 = 0. \tag{6c}$$

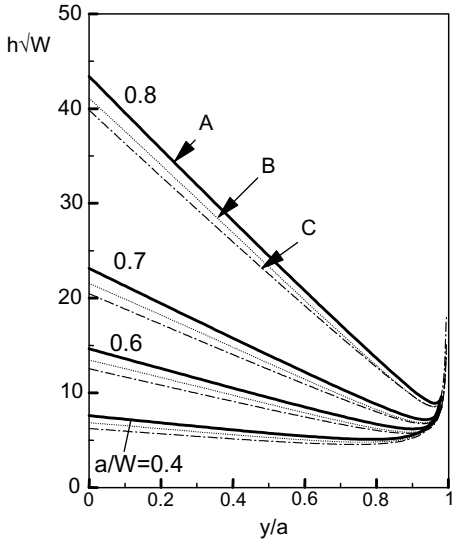

Fig. 2. Weight function for a fully graded plate with an external crack: (A) transition function Eq. (8a); (B) homogeneous material; and (C) transition function Eq. (8b).

From these three equations, the coefficients follow as

$$D_1 = \frac{35}{16}\sqrt{\frac{2\pi}{a}}\frac{K_\sigma}{\sigma} - \frac{15}{16}\sqrt{2\pi a}\frac{K_P}{P} - 7 \tag{7a}$$

$$D_2 = -\frac{35}{12}\sqrt{\frac{2\pi}{a}}\frac{K_\sigma}{\sigma} + \frac{15}{8}\sqrt{2\pi a}\frac{K_P}{P} + \frac{25}{3} \tag{7b}$$

$$D_3 = \frac{35}{48}\sqrt{\frac{2\pi}{a}}\frac{K_\sigma}{\sigma} - \frac{7}{16}\sqrt{2\pi a}\frac{K_P}{P} - \frac{7}{3}. \tag{7c}$$

In Fig. 2, weight functions are given for a homogeneous material and for two gradation functions: homogeneous material, part C is transition function in Eq. (8b).

$$\text{A}: \qquad E(y) = E_0\left(1 - \frac{y}{2W}\right) \tag{8a}$$

$$\text{C}: \qquad E(y) = E_0\left(1 + \frac{y}{W}\right) \tag{8b}$$

where W is the length of the plate in y-direction. It can be seen that for this linear change in the Young's modulus by a factor of two, only a small deviation from the weight function occurs for a homogeneous material.

The crack opening displacement $u(a, y)$ for given stress distribution follows from Eq. (2) as

$$u(y, a) = \int_y^a \frac{h(y, a') K(a')}{E(a')} da'. \tag{9}$$

Introducing Eq. (1) leads to

$$u(y, a) = \int_x^a \frac{h(y, a')}{E(a')} \left[\int_0^{a'} \sigma(y) h(y, a') dy \right] da'. \tag{10}$$

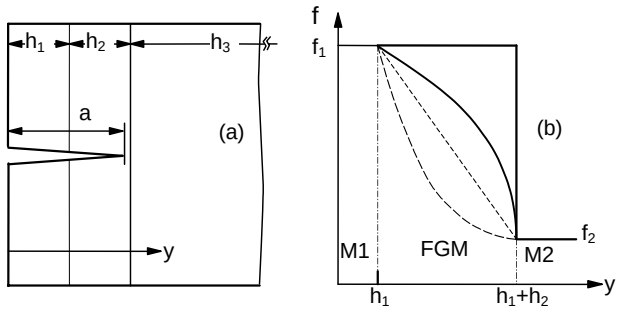

Fig. 3. (a) Crack in a plate with a graded interlayer; and (b) graded functions in the interlayer; M1, M2: homogeneous materials.

2.2. Stress intensity factor in a material with a graded interlayer under thermal loading [41]

A joint with a graded interlayer between two materials is considered, which is subjected to a change in temperature ΔT from the stress-free state (Fig. 3). The thickness of the two materials is h_1 and h_3, the thickness of the interlayer h_2. It is assumed that the Young's modulus E and the thermal expansion coefficient α follow the same gradation function, whereas the Poisson's ratio is assumed to be constant. The relation

$$f(x) = f_2 - (f_2 - f_1)\left(\frac{h_2 - y}{h_2}\right)^n \tag{11}$$

is used for E and α with $n = 1/2$, 1 and 2. The normalized stress σ_x in the uncracked joint is shown in Fig. 4 for $\alpha_1/\alpha_2 = 0.5$, $E_1/E_2 = 2$, $h_3/H = 0.05$ and $h_1/H = 0.125$ ($h_1 + h_2 + h_3 = H$). There is a continuous transition in the stresses. The stresses in the top layer are higher than in the ungraded joint. In Fig. 5, the normalized stress intensity factor is plotted versus the crack length. As can be expected from the stress distribution in the uncracked joint, the stress

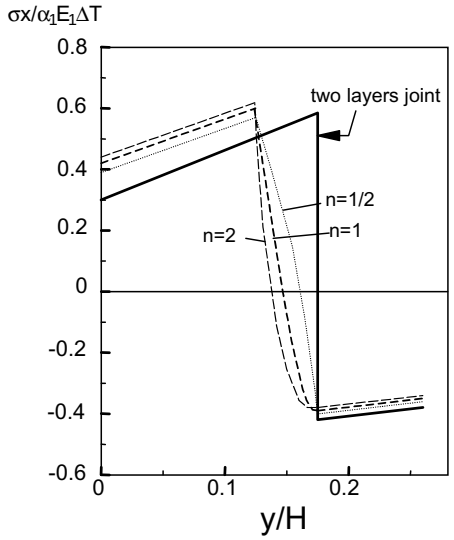

Fig. 4. Normalized stress distribution in the uncracked joint.

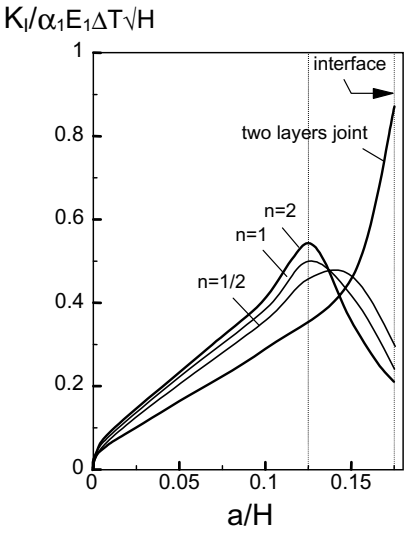

Fig. 5. Normalized stress intensity factor for joints with a graded interlayer.

intensity factor in the joint with a graded interlayer is higher for small cracks compared with the ungraded joint. If the cracks are growing into the graded layer the stress intensity factor decreases, whereas the stress intensity factor in the ungraded joint increases as the crack approaches the interface. In Fig. 6, the normalized stress intensity factors are compared for three joints: A, bimaterial with $h_1/H = 0.05$; B, joint with a graded interlayer of thickness $h_3/H = 0.05$ and $h_1/H = 0.05$ (grading function with $n = 1$); C, bimaterial joint with $h_1/H = 0.1$. For the joints A and C, the stress intensity factor increases as the crack approaches the interface. When comparing the joints A and B, it can be seen that in the top layer the stress intensity factor is lowered by introducing a graded interlayer. In the graded interlayer itself, however, the stress intensity factor is higher.

These examples show that a detailed discussion is necessary for an assessment of the benefit of a graded interlayer.

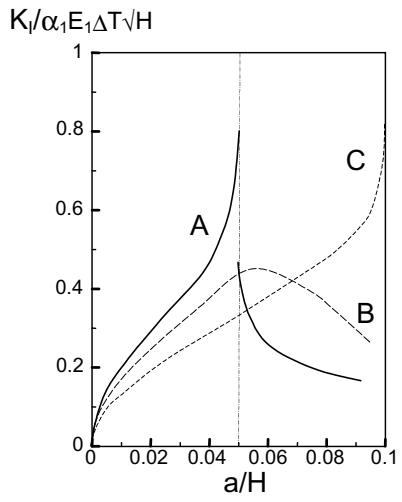

Fig. 6. Normalized stress intensity factors for three joints.

In a bimaterial with $E_1/E_2 > 1$, the stress intensity will exceed the fracture toughness, if the crack approaches the interface. Then, the crack may arrest at the interface because of the lower K in material 2 or the crack may kink and extend along the interface. In the graded material the stress intensity factor may always be below the fracture toughness, if a suitable grading function is selected. The gradation also affects subcritical crack extension. Under thermal fatigue loading, the crack growth rate da/dN depend on the range of the stress intensity factor ΔK, which can be described by the Paris-relation

$$\frac{\mathrm{d}a}{\mathrm{d}N} = C(\Delta K)^n \tag{12}$$

The parameters C and n depend on the material and are, therefore, a function of y. By integration of Eq. (12) from an initial to a critical crack size, the number of cycles to failure can be obtained. A possible beneficial effect depends on the distribution of K and the material parameters along the crack path.

Based on these considerations, a beneficial effect of a graded interlayer on the crack growth behavior may be possible, but has to be evaluated for each specific problem.

2.3. Rising crack growth resistance curve in gradient materials

In ceramic materials the resistance against crack extension increases with increasing crack extension. For most materials this effect is caused by crack border interaction behind the crack tip due to frictional contact of the crack borders or unbroken islands. This crack border interaction can be described by compressive stresses $\sigma_{\mathrm{br}}(y)$ acting along the crack border and leading to a negative stress intensity factor $K_{\mathrm{br}}(a)$. The stress intensity factor at the crack tip K_0 is the superposition of $K_{\mathrm{br}}(a)$ and

$$K_{\mathrm{appl}}(a) = \sigma\sqrt{a}Y\left(\frac{a}{W}\right). \tag{13}$$

For homogeneous materials, the crack extends at constant K_0 and, therefore, K_{appl} increases to compensate the increase of the negative K_{br}. The "bridging stress" of a homogeneous material is a unique function of the crack opening displacement u:

$$\sigma_{\mathrm{br}} = \sigma_{\mathrm{br}}(u)$$

The crack growth resistance curve—$K_{\mathrm{appl}} = K_{\mathrm{R}}$ as a function of the crack extension Δa is not an unique curve. The relation depends on the initial crack size and the stress distribution in the uncracked component.

In a gradient material, the critical stress intensity factor at the onset of crack extension K_0 and the relation between σ_{br} and the crack opening displacement depend on y:

$$K_0 = K_0(y), \qquad \sigma_{\mathrm{br}} = \sigma_{\mathrm{br}}(u, y)$$

The crack growth resistance curve can be obtained from the relation measured between the external load or stress applied and the crack extension by using Eq. (11) with $Y(a/W)$ for the specific gradient function $E(y)$. On the other hand, the crack growth resistance curve can be calculated from the known relations $K_0(y)$ and $\sigma_{\mathrm{br}}(y, u)$ by applying the relations

$$u_{\mathrm{total}} = u_{\mathrm{appl}} + u_{\mathrm{br}}$$

$$\sigma_{\mathrm{total}} = \sigma_{\mathrm{appl}} + \sigma_{\mathrm{br}}$$

and Eq. (10):

$$u_{\mathrm{total}}(y, a) = \int_y^a \frac{h(y, a')}{E(a')}\left[\int_0^{a'} \sigma_{\mathrm{br}}(u_{\mathrm{total}}, y)h(y, a')\mathrm{d}y\right]\mathrm{d}a' + \int_y^a \frac{h(y, a')}{E(a')}\left[\int_0^{a'} \sigma_{\mathrm{appl}}(y)h(y, a')\mathrm{d}y\right]\mathrm{d}a' \tag{14}$$

$$K_{\mathrm{appl}} = \sigma_{\mathrm{appl}}\sqrt{a}Y\left(\frac{a}{W}, y\right) = K_0(y) + K_{\mathrm{br}}(y) = K_0(y) + \sigma_{\mathrm{br}}\sqrt{a}Y\left(\frac{a}{W}, y\right). \tag{15}$$

This equation has to be solved iteratively.

Another problem is the determination of the bridging stresses as a function of the crack opening displacement. For a given initial crack length and applied stress, the bridging stresses can be obtained as a function of the distance behind the crack tip $\sigma_{\mathrm{br}}(y)$ from measurements of the crack opening displacement $u_{\mathrm{measured}}(y, a) = u_{\mathrm{total}}(y, a)$ at an applied stress $\sigma_{\mathrm{appl}}(y)$. Eqs. (10) and (14) can be written in the form of

$$u_{\mathrm{br}}(y, a) = u_{\mathrm{measured}}(y, a) - \int_y^a \frac{h(y, a')}{E(a')}\int_0^{a'} \sigma_{\mathrm{appl}}(y)h(y, a')\,\mathrm{d}y\,\mathrm{d}a' = \int_y^a \frac{h(y, a')}{E(a')}\int_0^{a'} \sigma_{\mathrm{br}}(y)h(y, a')\,\mathrm{d}y\,\mathrm{d}a' \tag{16}$$

From one measurement of the crack opening displacement for one crack length $a = a_0 + \Delta a$ and one applied load or $\sigma_{\mathrm{appl}}(y)$, the unknown function $\sigma_{\mathrm{br}}(y)$ can be obtained. In a diagram of σ_{br} versus the crack opening displacement with the coordinate x as a parameter, this leads to one point for each curve. The complete relation $\sigma_{\mathrm{br}}(y, u)$ can be obtained from measurements with different external loads or different crack extensions Δa applied.

As an example results of Neubrand et al. [42] are shown for an alumina/aluminum gradient material. First, σ_{br}–u-relation was determined from measurements of the crack opening displacement of compact tension specimens of a homogeneous material with 27% Al. In Fig. 7, the measured crack opening displacement u_{measured}, the calculated one for the applied load u_{appl}, and the difference of both u_{br} are plotted versus the distance behind the crack tip. Applying Eq. (16) with a constant Young's modulus, the bridging stress as a function of the distance behind the crack tip

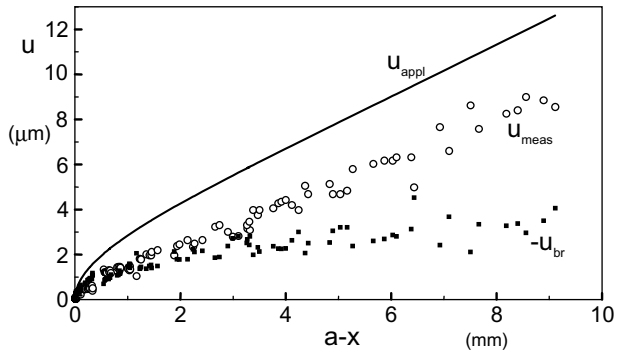

Fig. 7. Measured and calculated crack opening displacement (Al/Al_2O_3 with 27% Al).

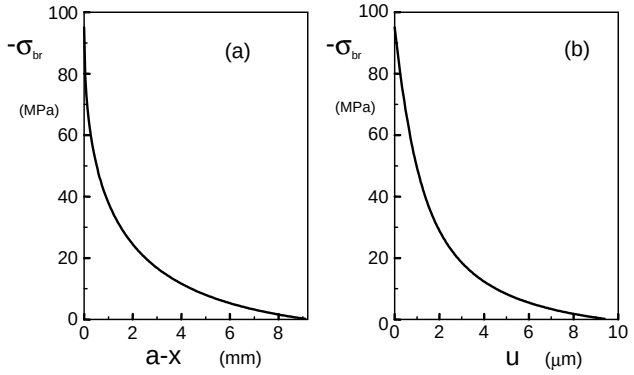

Fig. 8. Bridging stress vs.: (a) distance from crack tip; and (b) crack opening displacement (Al/Al_2O_3 with 27% Al).

is obtained as shown in Fig. 8a and the σ_{br}–u-relation as shown in Fig. 8b.

Fracture mechanics tests were performed using the compact tension specimens with three different grading functions shown in Fig. 9. The stress intensity factor was calculated from the load and the corresponding crack length by applying a relation given in [43]. The results are shown in Fig. 10. There is a significant effect of the grading function on the crack growth resistance curve. In addition predictions of the K_R curves were made from the σ_{br}–u-relation. For the gradient material, it was assumed that the relation between

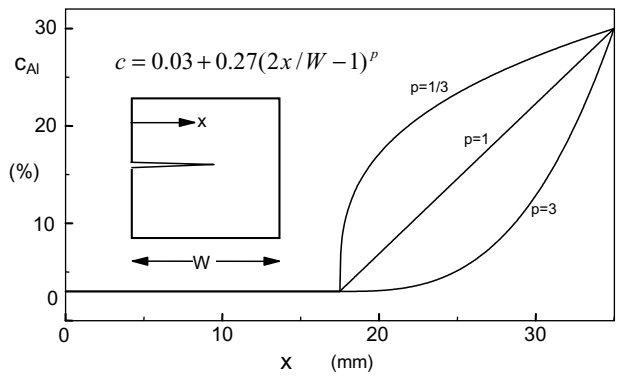

Fig. 9. Grading functions of a CT-specimen.

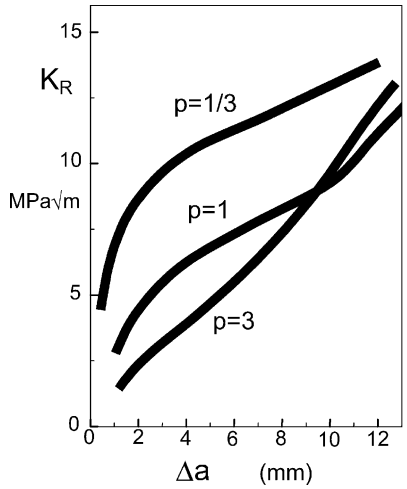

Fig. 10. Measured crack growth resistance curves for three different gradation functions.

the bridging stress and the crack opening displacement for different compositions is given by

$$\sigma_{br}(u, composition) = c_{Al}\, p(u),$$

where c_{Al} is the relative content of aluminum in the material and $p(u)$ taken from Fig. 8b. Based on the experimental results, the change of the stress intensity factor at the initiation of crack extension was assumed as to be

$$K_0 = 2.3 + 10.7 c_{Al}\left[\mathrm{MPa}\sqrt{m}\right]$$

In Fig. 11, the experimentally determined and the calculated crack growth resistance curves are compared. In a second calculation the effect of the residual stresses in the graded plates as determined by a finite element analysis (see Fig. 12) was considered. The stress intensity factor of the residual stresses was calculated according to

$$K_{res} = \int_0^a \sigma_{res}(y) h(y, a)\, dy.$$

Then the crack growth resistance curve is calculated as

$$K_{appl} = K_0 - K_{res} - K_{br}.$$

Comparing the different curves in Fig. 11 shows that there is a fairly good agreement between the directly obtained curves (thick lines) and the curves calculated from the bridging relation.

2.4. Determination of residual stresses in gradient materials

Gradient materials contain residual stresses due to the processing conditions. It is possible to determine these residual stresses from measurements of the crack opening displacement. The procedure is as follows: notches of different length are cut in the direction of gradation. The crack opening dis-

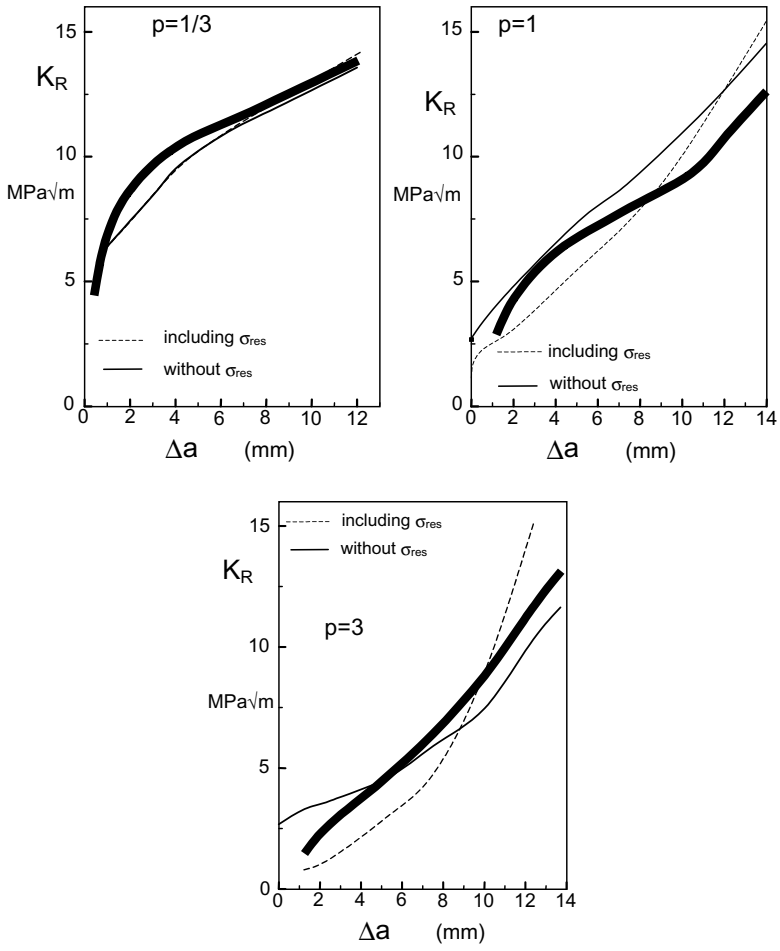

Fig. 11. Comparison of measured and calculated crack growth resistance curves.

placement is measured at the crack mouth. The crack opening displacement is given by

$$u_{\mathrm{res}} = \int_y^a \frac{h(y,a')}{E(a')} \left[\int_0^{a'} h(y,a')\sigma_{\mathrm{res}}(y)\mathrm{d}y \right] \mathrm{d}a'. \quad (17)$$

To solve this equation, the residual stresses are described a polynomial expression:

$$\sigma_{\mathrm{res}} = \sum_{i=0}^{n} A_i y^i. \quad (18)$$

Inserting Eq. (18) into Eq. (17) leads to:

$$u_{\mathrm{res}} = \sum_{i=0}^{n} A_i C_i \quad (19)$$

with

$$C_i(y) = \int_y^a \frac{h(y,a')}{E(a')} \left[\int_0^{a'} h(y',a')y'^i \mathrm{d}y' \right] \mathrm{d}a'. \quad (20)$$

Eq. (19) is a linear system of equations, which has to be solved for n measured crack opening displacements with n different notch depths.

As an example, a result obtained by Neubrand et al. [44] is presented. In the same material as described in Section 2.3, the crack opening displacement was measured near the surface of the specimen for notches with different depths. The residual stress distribution calculated from these COD measurements are shown in Fig. 12. These results are compared with finite element calculations considering cooling from 600 °C.

3. Reduced delamination in graded TBCs

3.1. Principle of optimizing gradients

Thermal barrier coatings (TBCs) with superior heat resistance are applied for gas turbine engine blades with to increase the energetic efficiency by running at higher operating temperature. The service life of TBCs is limited by spalling fracture [45]. Application of functionally graded TBCs with improved resistance against delamination and spalling is expected to extend service life. The strategy of graded TBC optimization is outlined in Fig. 13. It represents an extension of the scheme proposed in [46].

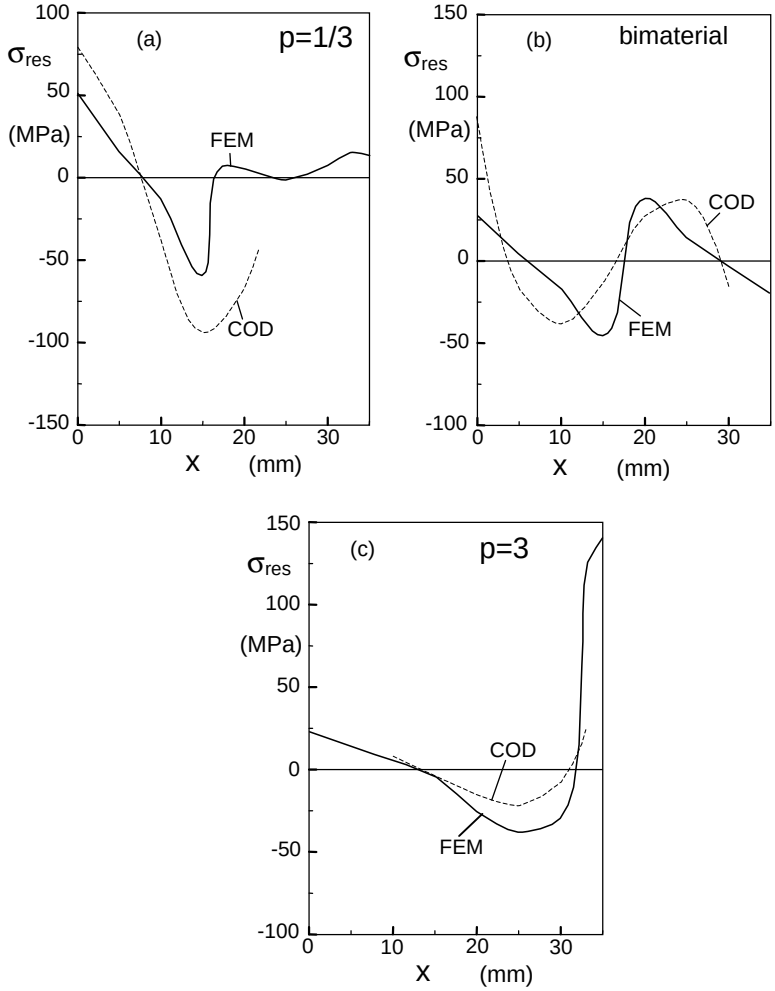

Fig. 12. Comparison of measured and calculated residual stresses.

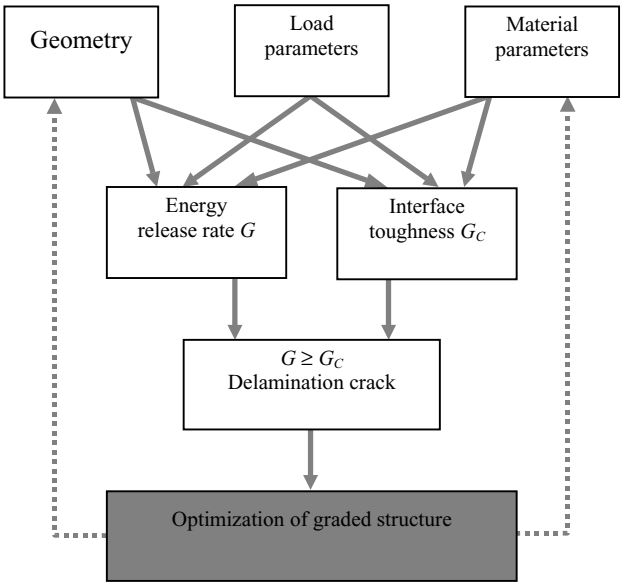

Fig. 13. Principle of optimizing gradients.

The concept of mixed mode crack propagation in layered materials [47] is used in combination with the conventional crack propagation criterion based on the strain energy release rate G and the interface toughness G_C. With the parameters of geometry, loading conditions, and material properties being given, displacements, strains, stresses, and, finally, the energy release rate G can be calculated for the given configuration. The interface toughness G_C which is a given material constant in simplest fracture mechanical problems is influenced by various factors, such as TBC manufacture and operating conditions, mode mixity of loading, and the transition function in this complex case of a layered structure.

The delamination crack is assumed to obey the conventional crack propagation criterion

$$G \geq G_C, \tag{21}$$

which means that it propagates if the energy release rate G exceeds its critical value G_C. TBCs modified by grading in such a way that G is always below G_C would withstand more severe conditions without damage. The potential effect of grading on both decreasing G and increasing G_C, with

the aim of a reduction of TBC damage is discussed in the papers [46,48,49].

Two series of experiments have been carried out in connection with our investigations aimed at understanding the basic mechanisms of TBC fracture and checking the usefulness of the present approach. One series involves cyclic surface heating by means of a laser beam. Another series involves various thermal loading regimes and a subsequent four-point bending test modified by a stiffening layer. It was demonstrated previously that cyclic surface heating by laser irradiation is a suitable test for the performance of non-graded and graded TBCs [46,50–52]. Such an experiment is suitable for studying the progress of damage and also for comparing the performance of non-graded and graded TBCs. The four-point bending test modified by a stiffening layer has proved suitable for investigating the influence of grading and aging on interface fracture toughness. These experiments and related finite element computations serve to understand and quantify the progress of TBC damage with a number of cycles and explain in which way grading may reduce or prevent this damage.

3.2. Graded TBC with increased interface toughness

Interface fracture toughness was measured on samples prepared by DLR Köln by means of electron-beam physical vapor deposition (EB-PVD). The non-graded samples were flat Nimonic plates with about 100 μm NiCoCrAlY bond coat and 250 μm partially stabilized ZrO_2. The graded samples contained a 50 μm intermediate layer between the bond coat and ZrO_2, with a graded transition from Al_2O_3 to ZrO_2 [53].

Interface toughness G_C was measured in a four-point bending test [54] modified by a stiffening layer [46,48,55,56] (Fig. 14). Results of non-graded and graded TBCs are listed in Table 1 for three kinds of samples differing by the degree of aging: as received (without aging); 100 h aged at 1000 °C; and 10 h aged at 1100 °C in air. These results clearly demonstrate two effects: aging at high temperature reduces G_C, as reported also in [57] for plasma sprayed coatings; and the introduction of a graded Al_2O_3 oxidation barrier between zirconia and the bond coat causes G_C to increase.

Table 1
Results of G_C measurement[a]

G_C (N/m)	Non-graded EB–PVD–TBC	Graded EB–PVD–TBC
Without aging	>81[b]	>81[b]
100 h at 1000 °C	63	>81[b]
10 h at 1100 °C	37	45

[a] [51].
[b] In these cases, there was no TBC failure, but a detachment of the stiffening layer.

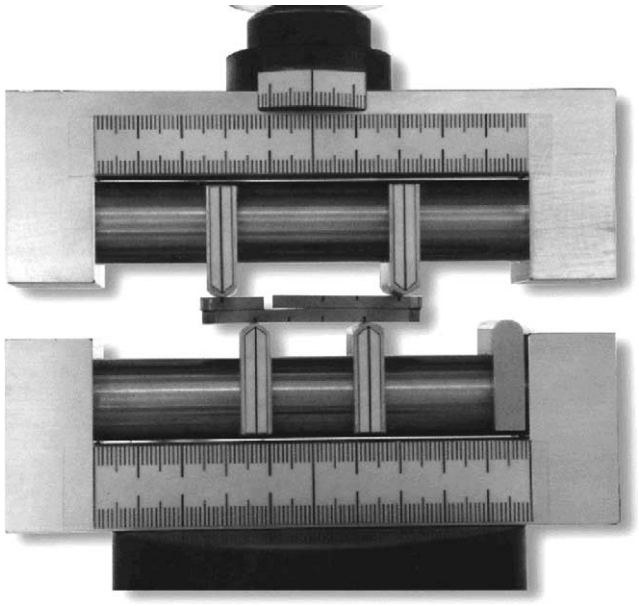

Fig. 14. TBC delamination testing equipment.

3.3. Laser-induced TBC damage

Intensive cyclic surface heating by means of laser irradiation is a suitable test for the analysis of TBC damage evolution [46,50–52,58]. It can be effectively applied for comparing the performance of non-graded and graded TBCs [51] for a wide range of temperatures and numbers of cycles. In these experiments the sample surface is locally heated by a 1 kW Nd-YAG laser beam, as shown in Fig. 15. The beam is deflected by two synchronized oscillating mirrors in such a way that a circular area on the sample surface is heated. The surface temperature is measured by a high-speed pyrometer combined with another oscillating mirror. The start of the crack can be detected by an acoustic sensor. A typical cycle consists of two phases: active heating for 1 and 10 s interval (see Fig. 16). The number

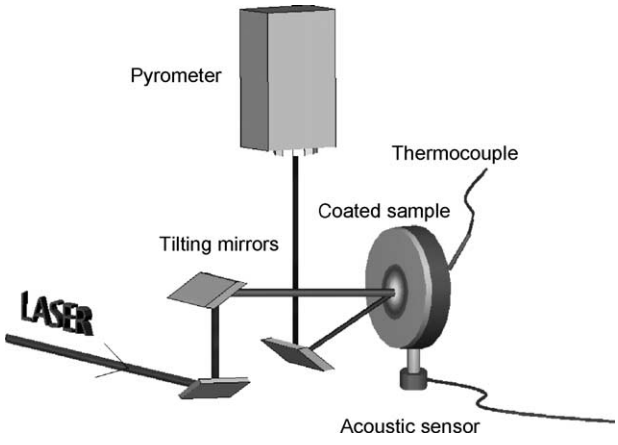

Fig. 15. Set-up of the laser heating experiment.

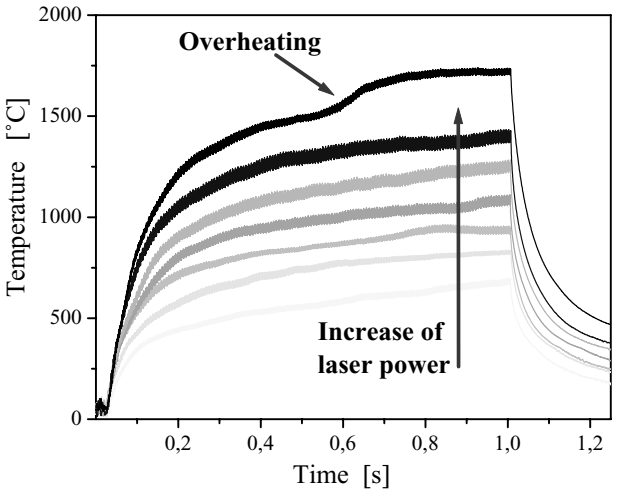

Fig. 16. Thermal cycling: part of an 11 s cycle, heating phase 1 s, and cooling phase 10 s.

of cycles per sample varies between several tens to several thousands. The maximum surface temperature employed is about 1600 °C.

TBC damage was investigated by microscopy and metallographic cuts. TBC failure was found to proceed in clearly distinguishable consecutive stages, as shown in Fig. 17. Note that N and T_{max} have was varied. There is no visible damage after 11 cycles for all TBCs. Short vertical cracks are observed after 30 cycles with $T_{max} = 1500\,^{\circ}C$ in the non-graded TBC (Fig. 17a) and after 300 cycles with $T_{max} = 1530\,^{\circ}C$ in the graded TBC (see Fig. 17d). Long vertical cracks and delamination arise after 1400 cycles at 1500 °C in the non-graded TBC (see Fig. 17b) and after 300 cycles at 1600 °C in the graded TBC (see Fig. 17f). Under the above loading conditions, local spalling is observed for non-graded TBC only.

It can be concluded that TBCs respond to thermal cycling of increasing severity with the following sequence of phenomena:

vertical cracks → delamination → blistering → spalling.

The onset of the stages of damage is delayed by grading. This experimental evidence can serve as a guidance for the following analytical and numerical fracture mechanics analysis aimed at optimizing the effect of grading.

Since, in the present experiments, damage depends on two parameters, N and T_{max} only, it can be conveniently represented by damage maps as in Fig. 18. Apparently, a graded interlayer delays delamination and subsequent further damage. Blistering and spalling have been identified visually. Delamination was detected by pyrometry. It is reflected by a sudden rise of the surface temperature. The kink in the upper curve of Fig. 16 is related to a sudden increase of thermal flow resistance due to delamination.

The following fracture mechanics modeling intends to reproduce an essential feature of the damage map, namely, the slope of the line indicating the critical damage threshold, by taking into account the variability of both G and G_C with N. The same subject was studies in [59] for atmospheric

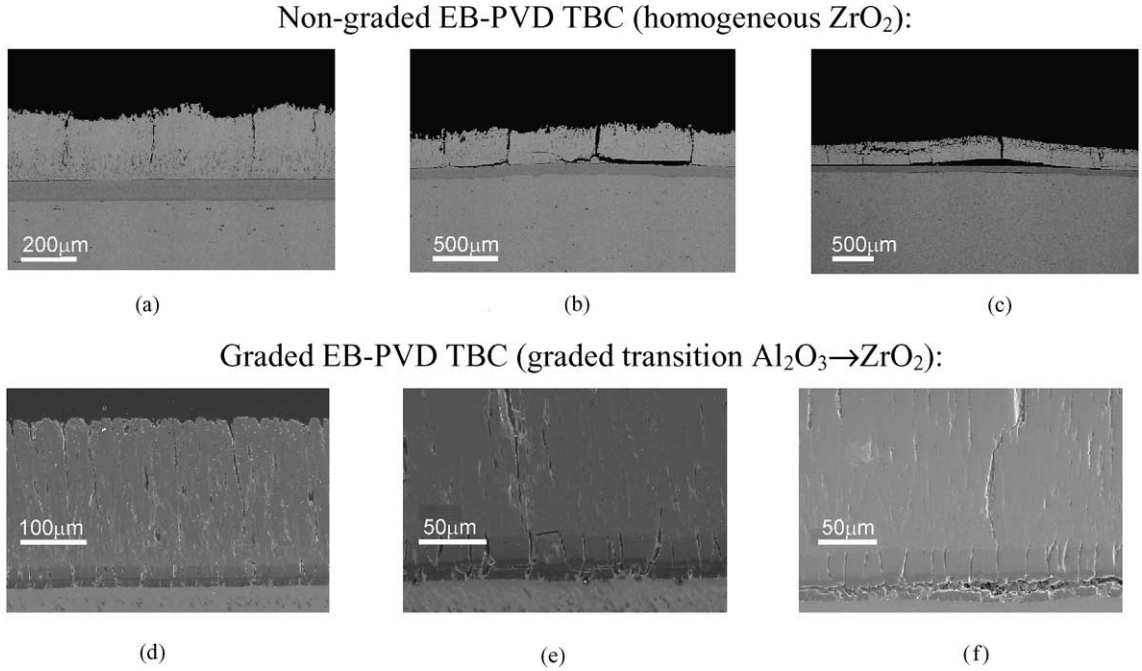

Fig. 17. Progress of damage in non-graded and graded TBCs [51] N and T_{max} denote the number of cycles and maximum surface temperature. For non-graded EB-PVD TBC (homogeneous ZrO_2): (a) $N = 30$, $T_{max} = 1500\,^{\circ}C$; (b) $N = 1400$, $T_{max} = 1500\,^{\circ}C$; and (c) $N = 900$, $T_{max} = 1600\,^{\circ}C$. For graded EB-PVD TBC (graded transition: $Al_2O_3 \rightarrow ZrO_2$): (d) $N = 300$, $T_{max} = 1530\,^{\circ}C$; (e) $N = 1000$, $T_{max} = 1530\,^{\circ}C$; and (f) $N = 300$, $T_{max} = 1600\,^{\circ}C$.

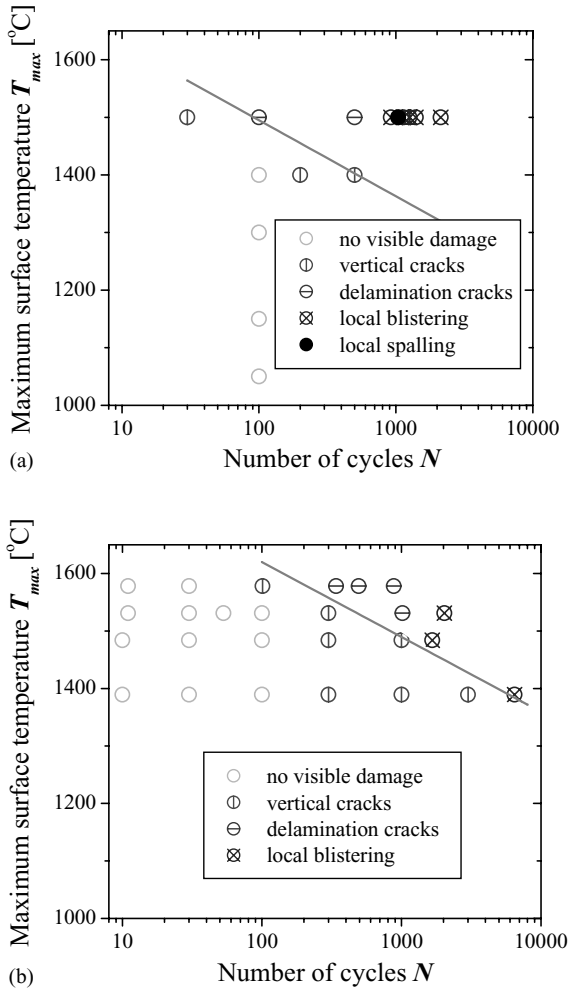

Fig. 18. Damage maps of cyclically heated: (a) non-graded; and (b) graded TBCs [51].

plasma-sprayed ZrO_2 coatings, where time-dependent safety maps served as an appropriate representation. The TBC failure process was discussed in this sense in [60], where an increase of interface stress and degrading of bond strength with time and number of cycles was analyzed in connection with the expected life time before the onset of spalling.

The higher damage resistance of graded TBC as compared to non-graded TBC (compare curves in Fig. 18b and Fig. 18a) is apparently due to the higher G_C of graded TBC after aging under heating (see Table 1).

3.4. Shrinkage stresses as a driving force

During laser heating (Fig. 16) the TBC-layer is subjected to high compressive thermal stress leading to high-temperature creep deformation in addition to sintering. Both mechanisms cause a high tensile stress building up while cooling down to room temperature after cyclic heating. A similar mechanism was investigated in [61] for metallic (Ti, Al)N coatings under laser shock loading. Considerable

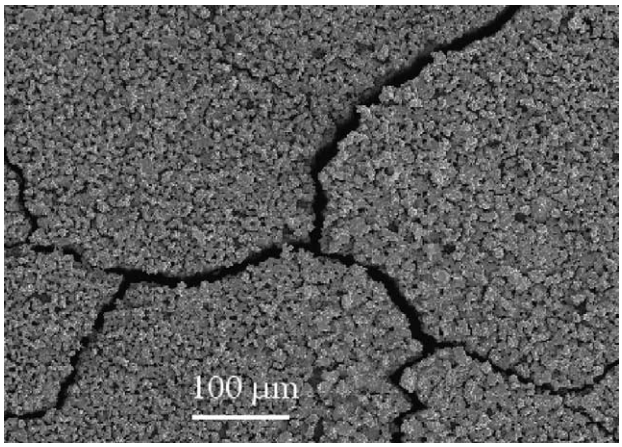

Fig. 19. Shrinkage cracks in thermally cycled TBC.

residual crack opening after cyclic heating (Fig. 19) indicates the presence of an average shrinkage strain of about 1%. Sintering of TBCs was discussed in [45,51]. Prolonged heating of TBC samples detached from the substrate by chemical dissolution of the NiCoCrAlY bond coat resulted in shrinkage strains of $\varepsilon_S \approx 1.4\%$ for 100 h at 1200 °C and $\varepsilon_S \approx 0.6\%$ for 250 h at 1050 °C (Fig. 20, curvature due to inhomogeneity of TBC). Progressive shrinkage due to sintering in thermal cycling increases the energy release rate for vertical cracks which subsequently turn into delamination cracks. (Note that the temperature needed for TBC damage in Fig. 17 is much higher because of the smaller total duration of laser heating with N cycles.)

3.5. Model for the analysis of delamination crack propagation

A simplified two-dimensional (plain strain) model is considered for the analysis of delamination cracks under thermal shock (Fig. 21a). Its symmetry allows the calculation to be restricted to a representative element with one crack only (Fig. 21b). Elastic isotropy is assumed, with E_1, ν_1,

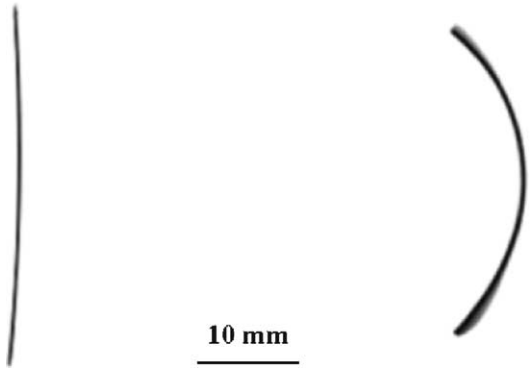

Fig. 20. Detached TBC: before (left) and after (right) deformation due to sintering for 100 h at 1200 °C.

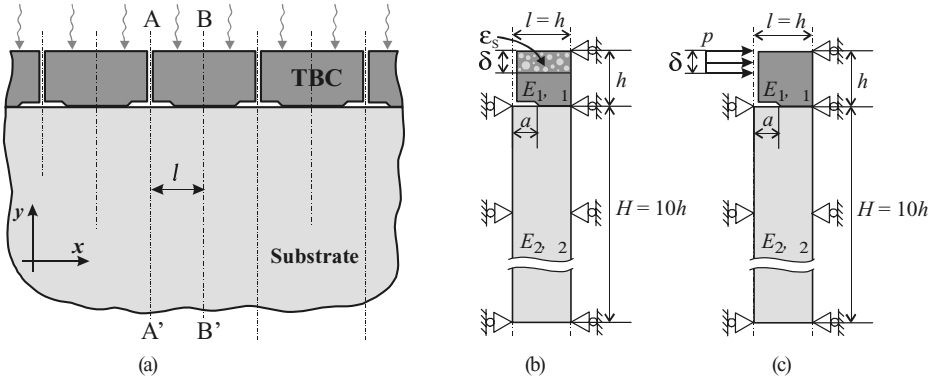

Fig. 21. Model for the analysis of delamination crack propagation due to sintering.

E_2, and ν_2 being the elastic constants for the TBC and the substrate, respectively. The sintering effect is characterized by two parameters: average shrinkage strain ε_S and depth δ (see also Fig. 21b).

3.6. FE modeling

Delamination crack propagation was computed by means of the finite element method (FEM). The finite element model corresponding to the problem depicted in Fig. 20b is shown in Fig. 22. The MARC finite element program package [62] was used for the calculation involving a 2D mesh of eight-noded isoparametric finite elements with four integration points for stiffness matrix computation. The number of elements varied with relative thickness h/H and dimensionless crack length a/l and reached about 1500. A highly refined self-similarly focused mesh was used in the vicinity of the crack tip. The size of the elements around the crack tip was about $h/680$. The depth of substrate H was taken as 10 h, which was sufficiently large to approximate half space. The representative element (Fig. 21b) was fixed horizontally on the right. Deviation of G due to this simplification did not exceed 8% compared to the case of periodic boundary conditions.

The energy release rate G is calculated using the J-integral via differential stiffness technique [62]. Accuracy of the model and methods considered is checked by comparison with the analytical result for homogeneous material within the limits of large l/h and $\delta/h = 1$: $G_{SS} = (1-\nu_1^2)p^2h/(2E_1) = (1+\nu_1)/(1-\nu_1)E_1\varepsilon_S^2h/2$ (Eq. (22)).

In this model, the effect of sintering is simulated by assuming a homogeneous initial strain ε_S in an upper stratum of depth δ of the TBC (see Fig. 21b). As another check of the numerical computations, the equivalent problem of external pressure: $p = E_1\varepsilon_S/(1-\nu_1)$ applied to the boundary (see Fig. 21c) is calculated as well. The coincidence of the

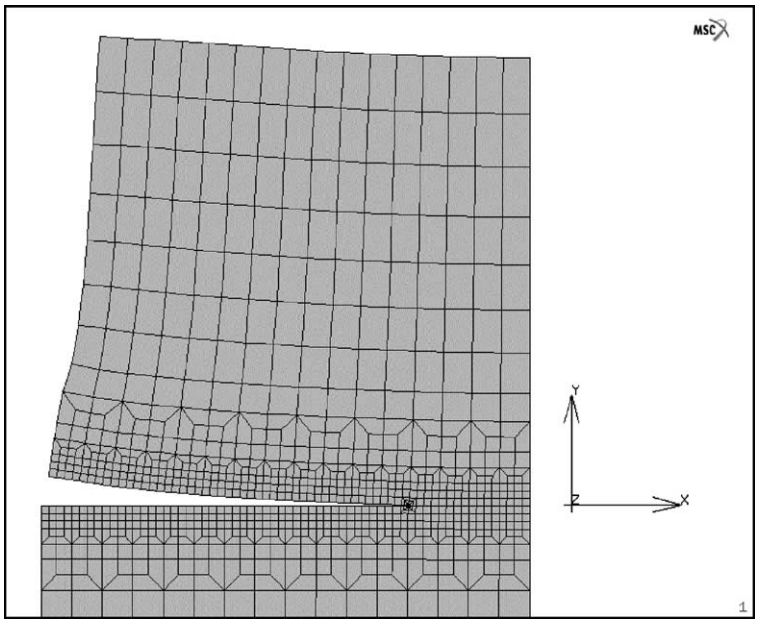

Fig. 22. Delamination crack propagation caused by sintering ($\varepsilon_s = 0.4\%$, $\delta/h = 0.8$, $a/l = 0.75$). Displacements 20 times magnified.

results turns out to be better than <0.5%, thus proving the consistency of the calculations.

Delamination is analyzed on the basis of elastic finite element solutions for variable crack lengths and loading conditions. The crack configurations for $a/l = 0.75$ are shown in Fig. 22.

The deformations seen in Fig. 22 (20 times magnified) show that the upper layer experiences both opening and sliding relative to the substrate, thus indicating "mixed mode" conditions. Variation of G with crack propagation is given in Fig. 23 for various values of δ/h. The prominent feature of the $G(a)$ curves in Fig. 23 is the maximum, which is about 20–30% of the steady-state value G_{SS} of an equivalent specimen with infinite width l, which is defined by Eq. (22) as follows:

$$G_{SS} = \frac{1+\nu_1}{1-\nu_1}\frac{E_1\varepsilon_S^2 h}{2}\left(\frac{\delta}{h}\right)^2\left[1+3\left(1-\frac{\delta}{h}\right)^2\right]. \qquad (22)$$

The curves in Fig. 23 start from values of $G|_{a/l\to 0}$ for delamination cracks, which are defined by the energy release rate for a vertical crack. (In case of a homogeneous material, the energy release rate of the infinitesimal delamination kink is 1/4 of that of the vertical crack). The value of $G|_{a/l\to 0}$ may exceed G_{SS} at $\delta/h = 1$, and it depends strongly on the relative depth δ/h of the sintering zone. With further delamination crack propagation, G approaches the steady state value G_{SS}, but does not reach it, due to relatively small value of l. For $a \to l$ the energy release rate G approaches zero (convergent debonding by [63]). In view of these tendencies, the existence of a maximum in the $G(a)$ curves, as shown in Fig. 23, is obviously necessary. In contrast to δ/h, the loading parameter ε_S has no influence on $G(a)/G_{SS}$.

In reality, the geometry parameter l is more or less random. The experiments show that the average half distance between vertical cracks is about equal to the TBC thickness h. The value $l = 1.5\,h$ was assumed in [51]. G depends on l/h as shown in Fig. 24. (Note also the convergence of the curves for $a \to l$.) The case $l = h$ is considered here in detail. Natural randomness of l creates favorable conditions for spalling under certain combinations of loading parameters during cycling.

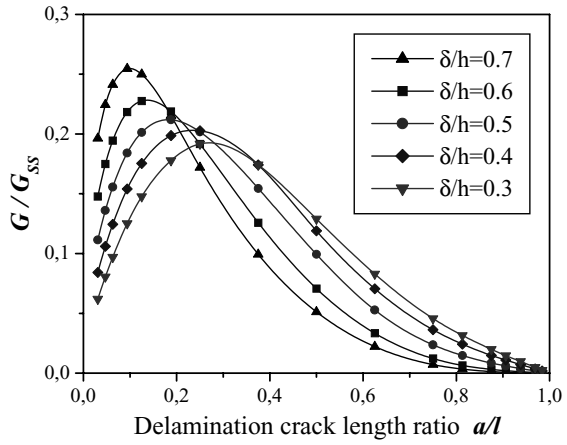

Fig. 23. Energy release rate vs. crack length for $l = h$. Analogous results for $l = 1.5\,h$ have been calculated in [51].

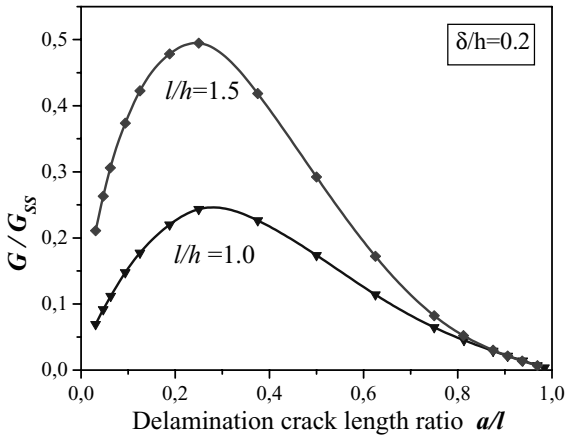

Fig. 24. Influence of crack net density parameter (l/h) on energy release rate curves alteration with crack propagation. The mutual unloading of vertical cracks leads to decreasing of G for lower l/h.

The peculiarities of the G behavior as revealed by the numerical simulations are the basis for the following analysis of TBC failure.

3.7. Delamination conditions

During cyclic laser beam heating, the shrinkage stress increases, and so does the energy release rate G. The numerical results of Fig. 25 were obtained under the assumption of a stress-free shrinkage strain $\varepsilon_S = 0.4\%$ and $\delta/h = 0.8$ for 100 h at 1000 °C ($G_{SS} = 209$ N/m), as suggested by the shrinkage evident in Figs. 19 and 20. (This thermal loading is the same as in Table 1, second line.) The computations were performed using the following Young's moduli: $E_1 = 85$ GPa, $E_2 = 215$ GPa, $\nu_1 = 0.177$, $\nu_2 = 0.3$ [64].

After 100 h at 1000 °C, G stays below G_C in the case of a graded TBC (Fig. 25b) and G exceeds G_C in the non-graded TBC so that the delamination crack is driven to $a/l \approx 0.1$ in Fig. 25a. At higher temperature T_{max} and number of cycles N, the value of G rises as a result of increasing shrinkage strain ε_S and depth δ (see Fig. 26). Furthermore, G_C is assumed to be reduced from 63 to 37 N/m (cf. Table 1, 1100 °C). If G exceeds the interface toughness G_C, unstable delamination sets in and proceeds to the position indicated by the solid arrow in Fig. 26 at least. Under continuing cyclic heating, G increases further and the delamination crack is pushed along in stable propagation as indicated by the dashed arrow. In this way, a delamination crack length of $a/l \approx 0.65$ is reached for the assumed values of $\varepsilon_S = 0.5\%$ and $\delta/h = 0.9$. (Note that the mode mixity angle ψ^* for the delamination crack in Fig. 23 was calculated in [51]. The dependence $G_C(\psi^*)$ was discussed briefly in [51]).

The described model can explain the delamination crack propagation with increasing ε_S and δ due to progressive

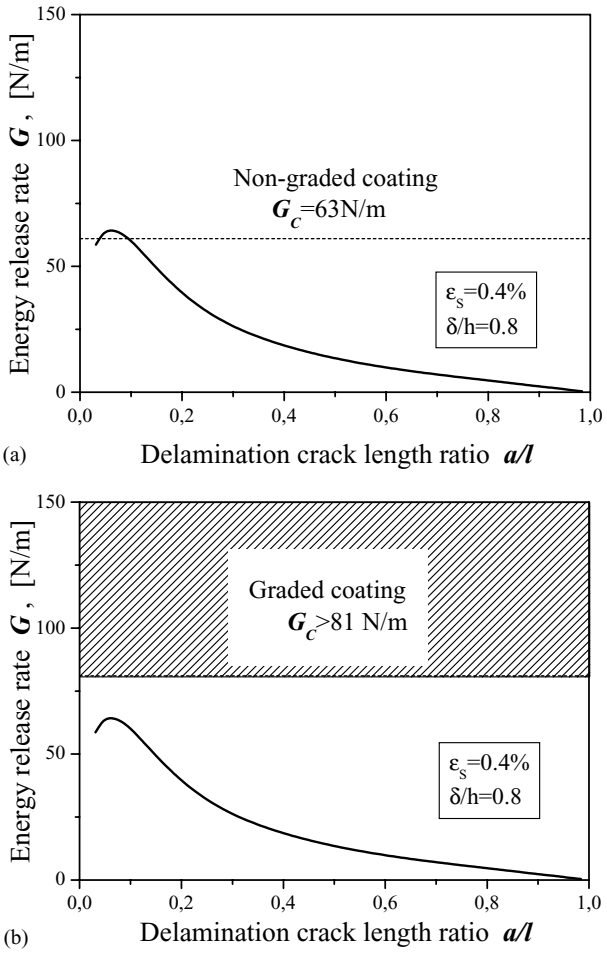

Fig. 25. Effect of grading on delamination crack propagation: (a) non-graded TBC (100 h, 1000 °C), $l = h$; and (b) graded TBC (100 h, 1000 °C), $l = h$.

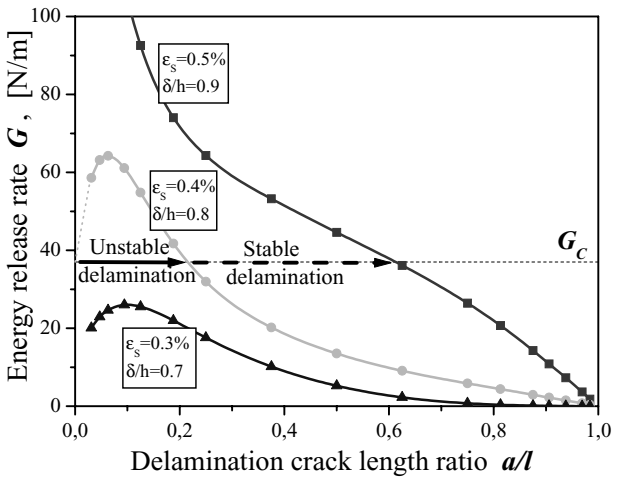

Fig. 26. Stable and unstable delamination with increasing ε_s and δ due to progressive sintering.

sintering. However, it is not quite obvious how spalling is brought about in the case of vertical cracks which do not close under heating. The energy release rate decreases with the approach of two adjacent delamination cracks so that delamination stops (Fig. 26). As a clue to the possible mechanism, spalling is observed during the heating stage of the cycle only (compare overheating in Fig. 16). These observations suggest that bending of the unilaterally attached flap due to transient heating may be the cause of final detachment. Based on this idea, a new model of spalling fracture is developed in [65].

4. Conclusions

The fracture mechanics analysis of cracks in functionally graded materials leads to the following results.

A graded interlayer does not necessarily lead to a reduction of the stress intensity factor. The weight function method can be applied to analyze the rising crack growth resistance in graded materials and calculate residual stresses after cooling from the process temperature.

A fracture mechanics analysis of the performance of graded and non-graded TBCs was carried out taking into account the multistage character of the TBC failure process. TBC damage resistance was tested by means of cyclic surface heating using laser irradiation. In this way, the influence of aging and grading on the performance of TBCs could be quantified. The observed sequence of TBC damage involved several stages: vertical cracking → delamination → blistering → spalling.

The fracture mechanics models proposed are aimed at explaining the essential feature of the damage map in Fig. 18, which is the downward slope of the critical damage curve. This slope is brought about by both the increase of shrinkage stress and the decrease of interface fracture toughness. Accordingly, the principle of graded TBC optimization is reduced to keeping G below G_C as well as possible.

An increase of interface fracture toughness G_C due to grading and a decrease due to aging was measured in a four-point bending test modified by a stiffening layer. The results of finite element modeling of the laser-induced TBC delamination process are compatible with the experimental data. Correlation with the damage observed in cyclic heating is discussed. It is explained in which way grading may occur to reduce the damage.

Acknowledgements

The authors thank the Deutsche Forschungsgemeinschaft (DFG) for support within the priority program “Gradientenwerkstoffe” and the Deutsches Zentrum für Luft- und Raumfahrt (DLR) Köln for supplying sample material.

References

[1] Y.Y. Yang, D. Munz, W. Schaller, Int. J. Fract. 87 (1997) L113–L118.
[2] A. Mortensen, S. Suresh, Int. Mater. Res. 40 (1995) 239–265.
[3] F. Bohner, J.K. Gregory, Mater. Sci. Forum 308–311 (1999) 313–318.
[4] M. Dong, L. Leßle, U. Weber, S. Schmauder, Mater. Sci. Forum 308–311 (1999) 1000–1005.
[5] S. Raßbach, W. Lehnert, Comput. Mater. Sci. 16 (1999) 167–175.
[6] W. Schäff, M. Hagenbruch, C. Körner, R.F. Singer, in: Proceedings of the ICCM-12, Paris, France, 1999, Paper no. 328.
[7] F. Delale, F. Erdogan, J. Appl. Mech. 50 (1983) 609–614.
[8] W.T. Ang, D.L. Clements, Int. J. Solid Struct. 23 (1987) 1089–1104.
[9] N. Noda, Z.-H. Jin, Int. J. Solid Struct. 30 (1993) 1039–1056.
[10] M. Ozturk, F. Erdogan, J. Appl. Mech. 60 (1993) 406–413.
[11] N. Konda, F. Erdogan, Eng. Fract. Mech. 47 (1994) 533–545.
[12] Z.-H. Jin, N. Noda, Int. J. Solid Struct. 31 (1994) 203–218.
[13] M. Ozturk, F. Erdogan, J. Appl. Mech. 116 (1995) 116–125.
[14] G. Bao, L. Wang, Int. J. Solid Struct. 32 (1995) 2853–2871.
[15] M. Ozturk, F. Erdogan, Int. J. Solid Struct. 33 (1996) 193–219.
[16] H.J. Choi, J. Appl. Mech. 63 (1996) 479–486.
[17] H.J. Choi, Int. J. Solid Struct. 3 (1996) 4101–4117.
[18] F. Erdogan, B.H. Wu, J. Therm. Stress. 19 (1996) 237–265.
[19] Z.-H. Jin, R.C. Barta, J. Therm. Stress. 19 (1996) 317–339.
[20] X. Wang, Z. Zou, D. Wang, Int. J. Fract. 82 (1996) 335–343.
[21] P. Gu, R.J. Asaro, Int. J. Solid Struct. 34 (1997) 1–17.
[22] P. Gu, R.J. Asaro, Int. J. Solid Struct. 34 (1997) 3085–3098.
[23] S. Kadioglu, S. Dag, S. Yahsi, Int. J. Fract. 94 (1998) 63–77.
[24] H.J. Choi, T.E. Jin, K.Y. Lee, Int. J. Fract. 94 (1998) 123–135.
[25] C. Li, Z. Zou, Fatige Fract. Eng. Mater. Struct. 21 (1998) 1447–1457.
[26] C. Li, Z. Zou, Int. J. Press. Vess. Pip. 75 (1998) 499–507.
[27] C. Li, Z. Zou, Z. Duan, Eng. Fract. Mech. 63 (1999) 735–749.
[28] N.I. Shbeeb, W.K. Binienda, Eng. Fract. Mech. 64 (1999) 693–720.
[29] P.R. Marur, H.V. Tippur, Int. J. Solid Struct. 37 (2000) 5353–5370.
[30] Y.-S. Chan, G.H. Paulino, A.C. Fannjiang, Int. J. Solid Struct. 38 (2001) 2989–3005.
[31] C. Cabrera, J. Reimanis, Eng. Fract. Mech. 69 (2002) 1667–1678.
[32] J.-H. Kim, G.H. Paulino, Eng. Fract. Mech. 69 (2002) 1557–1586.
[33] J.-H. Kim, G.H. Paulino, Int. J. Numer. Methods Eng. 53 (2002) 1903–1935.
[34] S. Dag, F. Erdogan, Eng. Fract. Mech. 69 (2002) 1729–1751.
[35] R.J. Moon, M. Hoffmann, J. Hilden, K.J. Bowman, K.P. Trumble, J. Rödel, Eng. Fract. Mech. 59 (2002) 1647–1665.
[36] J.R. Rice, Int. J. Solid Struct. 8 (1972) 751–758.
[37] T. Fett, D. Munz, Y.Y. Yang, Eng. Fract. Mech. 65 (2000) 393–403.
[38] T. Fett, D. Munz, Stress Intensity Factors and Weight Functions, Computational Mechanics Publications, Southampton, 1997.
[39] T. Fett, D. Munz, Y.Y. Yang, Fatige Fract. Eng., Mater. Struct. 23 (2000) 191–198.
[40] T. Fett, C. Mattheck, D. Munz, Eng. Fract. Mech. 27 (1987) 697–715.
[41] O. Bleeck, D. Munz, W. Schaller, Y.Y. Yang, Eng. Fract. Mech. 60 (1998) 615–623.
[42] A. Neubrand, T.-J. Chung, S. Lucato, T. Fett, J. Rödel, Mater. Sci. Eng. A, submitted for publication.
[43] T.-J. Chung, A. Neubrand, J. Rödel, T. Fett, in: K. Trumble, K. Bowman, I. Reimanis, S. Sampath (Eds.), Functionally Graded Materials 2000, American Ceramic Society Westerville, OH, Ceram. Trans. 114 (2001) 789.
[44] A. Neubrand, T.J. Chung, E.D. Steffler, T. Fett, J. Rödel, J. Mater. Res 17 (2002) 2912–2920.
[45] D.M. Nissley, NASA Confer. Publ. 3312 (1995) 265.
[46] I. Hofinger, H.-A. Bahr, H. Balke, G. Kirchhoff, C. Haeusler, H.-J. Weiss, Mater. Sci. Forum 308–311 (1999) 450.
[47] J.W. Hutchinson, Z. Suo, Adv. Appl. Mech. 29 (1991) 63.
[48] H. Balke, I. Hofinger, C. Haeusler, H.-A. Bahr, H.-J. Weiss, G. Kirchhoff, Arch. Appl. Mech. 70 (2000) 193.
[49] G. Bao, H. Cai, Acta Mater. 45 (1997) 1055.
[50] C.Y. Jian, T. Hashida, H. Takahashi, M. Saito, Composit. Eng. 5 (1995) 879.
[51] H. Balke, H.-A. Bahr, A.S. Semenov, I. Hofinger, C. Haeusler, G. Kirchhoff, H.-J. Weiss, in: Proceedings of the Sixth International Symposium on Functionally Graded Materials, Colorado, USA, 10–14 September 2000, 205.
[52] A. Kawasaki, R. Watanabe, M. Yuki, Y. Nakanishi, H. Onabe, Mater. Trans. (JIM37) 4 (1996) 788.
[53] T. Krell, U. Schulz, M. Peters, W.A. Kaysser, Mater. Sci. Forum 308–311 (1999) 396.
[54] P.G. Charalambides, J. Lund, A.G. Evans, R.M. McMeeking, J. Appl. Mech. 56 (1989) 77.
[55] I. Hofinger, M. Oechsner, H.-A. Bahr, M.V. Swain, Int. J. Fract. 92 (1998) 213.
[56] I. Pflugbeil, H.-A. Bahr, H. Balke, Technische Mechanik 17 (1997) 279.
[57] L.L. Shaw, Scripta Mater. 10 (1998) 1427.
[58] W. Pompe, H.-A. Bahr, I. Pflugbeil, G. Kirchhoff, P. Langmeier, H.-J. Weiss, Mater. Sci. Eng. A 233 (1997) 167.
[59] G. Thurn, G.A. Schneider, H.-A. Bahr, F. Aldinger, Surf. Coat. Technol. 123 (2000) 147.
[60] M. Gell, E. Jordan, K. Vaidyanathan, K. McCarron, B. Barber, Y.-H. Sohn, V.K. Tolpygo, Surf. Coat. Technol. 120–121 (1999) 53.
[61] K. Klotz, H.-A. Bahr, H. Balke, Th. Goebel, S. Menzel, U. Bahr, G. Kirchhoff, K. Wetzig, Thin Solid Films 413 (2002) 131.
[62] MARC, vol. A, version K7.3, MARC Analysis Research Corporation, 1999, p. 584.
[63] M.Y. He, A.G. Evans, J.W. Hutchinson, Acta Mater. 45 (1997) 3481.
[64] U. Schulz, DLR Köln, private communication, 1996.
[65] A.S. Semenov, H.-A. Bahr, H. Balke, H.-J. Weiss, Thin Solid Films, in press.